Proceedings of the International Association for
Shell and Spatial Structures (IASS) Symposium 2013
„BEYOND THE LIMITS OF MAN"
23-27 September, Wroclaw University of Technology, Poland
J.B. Obrębski and R. Tarczewski (eds.)

Study on Nonlinear Vibration Characteristics of RC/CFRC Arches by Vibration Tests and Simulations

Atsushi Mutoh[1], Shun Muramoto[2] and Akihiro Masuda[2]

[1] Professor, Department of Architecture, The Faculty of Science and Technology, Meijo University, Nagoya, Japan, amutoh@meijo-u.ac.jp
[2] Graduate Student, The Faculty of Science and Technology, Meijo University, Nagoya, Japan

Summary: In this paper, the results of a dynamic destructive experiment of a reinforced concrete (RC) arch and its numerical analysis for the purpose of evaluation of earthquake resistance of an RC arch/shell of a large span and verification of the numerical analysis technique are shown. In the test, an arch with a 20-m span was considered, and a circular arch of a 1/10 scale was used as the specimen. In order to reproduce the vibration destruction by using a seismic-wave input, an arch of comparatively small strength predicted by a prior numeric simulation was designed. In the experiment, input by a real seismic-wave record (JMA-Kobe), which gave time compression based on a similarity rule, was used on two levels after checking the natural frequency by a sweep test. The dynamic failure mode and the strength were identified by the experimental results, and a qualitatively and quantitatively good coincidence with a numerical simulation was obtained. In the test, although the structural instability, which results in four hinges, was prevented for safety, in a computational analysis, numerical instability was shown at the stage with three hinges. It is considered that a prediction with sufficient accuracy is practically possible. In addition, the reinforcement effects by a carbon fibre sheet were also examined.

Keywords: *reinforced concrete arch, ultimate strength, shaking table test, dynamic nonlinear analysis.*

1. INTRODUCTION

To concrete arch and shell, experimental, analytical and numerical analysis examination are tried about those deformation, damage, ultimate strength and failure mode by many past researches. In Japan, to the shell of the form of a cylinder, a circular, a cone, a hyperbolic, etc., the destructive experiment of a large number using scale reduction models are conducted from the 1950s to the present, and those arrangement is currently performed. In general, although these structures have a large load-carrying capacity, buckling and the influence of imperfections are always pointed out simultaneously. During their structural design, the existence of those indefinite elements serves as an important examination item about strength prediction or a setup of a safety ratio. In addition, in a country with frequent earthquakes, evaluation of the action to dynamic load is an important subject.

In this research, the dynamic destructive experiment for an RC arch is conducted, and the possibility of pursuing the phenomenon to a dynamic failure sate is verified by numerical analysis.

2. EXPERIMENTAL MODEL AND TESTING SYSTEMT

As regards the structural behaviour of an RC arch, material nonlinear characteristics and combined nonlinear characteristics by the existence of two or more equilibrium curves which originate geometrically nonlinear, are expected depending on its shape. In this research, a circular arch is subjected to examination. As shown in Fig. 1, the arch examined, has a span of 2m, and a rise-span ratio of 0.25; its two ends are pinned to a support, the section is set to a rectangle of 2.0×4.0 cm, and single reinforcement with 1.0%.

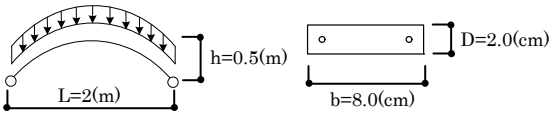

Figure 1: Experimental model of RC arch

2.1. Model set up by pre-test simulation

In the test, the 20m span circular arch was supposing and 1/10 scale was used as the specimen. In order to reproduce the vibration destruction by using a seismic-wave input, an arch of comparatively small strength predicted by a prior numeric simulation was designed. In the experiment, the input by a real seismic-wave record (JMA-Kobe), which gave the time compression based on a similarity rule, was used.

The Fourier spectrum of the time-compressed JMA-Kobe NS is shown in Fig. 2 along with the change in the natural frequency of the model as a function of the weight applied to it, and the result of the seismic response analysis of each model is summarized in Table 1.

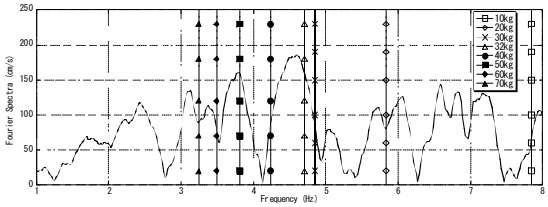

Figure 2 Change in the natural frequency with weight

Table 1 Estimation of dynamic failure for each weight

additional mass (kg/point)		10kg	20kg	30kg	32kg	40kg	50kg
natural period (s)		0.13	0.17	0.21	0.21	0.24	0.26
natural frequency (Hz)		7.84	5.83	4.85	4.71	4.24	3.81
JMA-Kobe	1-dir.(NS)	—	—	×	×	×	×
	2-dir. (NS+UD)	—	—	×	×	×	×

×; unstable during computation

A weight exceeding 30 kg caused the model to become unstable during time steps. It was assumed that under the influence of rigidity reduction such as that caused by the progress of cracks, the natural period of the specimen increased during a time response, and a value somewhat shorter than that corresponding to the peak of the spectrum of seismic waves was set up as the 1st natural period of the specimen. In the test, a 32-kg weight was set up. The free-vibration modes of the arch specimen and the corresponding frequencies are shown in Fig. 3.

(a) first mode (4.71Hz) (b)second mode (19.40Hz)

Figure 3 Free-vibration modes of the arch specimen

The estimated deformation modes at the time of the maximum response are shown in Fig. 6.

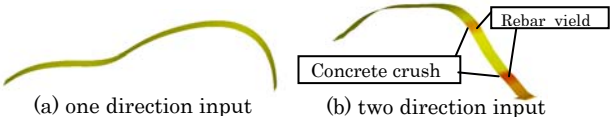

(a) one direction input (b) two direction input

Figure 4 Estimated deformation modes at the peak response

In the pre-test simulation, after the maximum response, an acceleration of about 750- cm/s2 (in the level direction) and 900 cm/s2 (in the vertical direction) was observed, a result in which an arch collapses was brought. In addition, the influence of an up-down input showed the result to which imperfection assume relates.

2.2. Testing system

The system image of the shaking table test of an RC arch, which receives two-direction input, and an actual situation are shown in Fig. 5.

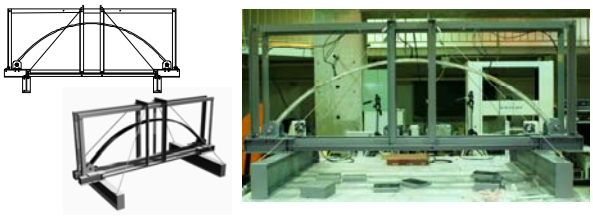

Figure 5 System for vibration testing of RC arch

2.2.1. Specimen

While manufacturing an examination object, in order to control the geometric imperfections, a mold that continuously transferred the entire sheet was used (Fig. 6). The portions of the pinned supports were manufactured by inserting a core stick in the pipe embedded on the specimen, and the ends were reinforced by increasing the thickness and installing a steel mesh.

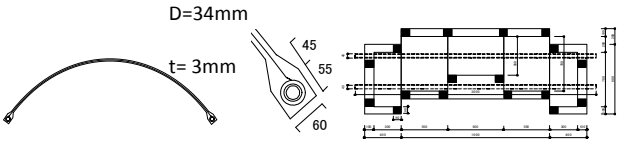

overall geometry end detail mold with imperfection control

Figure 6: Details of specimen and mold system

2.2.2. Additional weight and initial imperfection

A total of eight additional weights (4kg/sheet) were fixed at two locations on the specimen with the help of bolts. Before the experiment, the errors in the shape and thickness were precisely measured. Installation of weights and the measurement result of geometric imperfection are shown in Fig. 7.

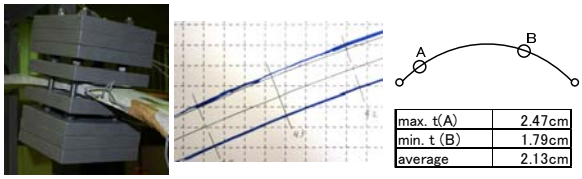

(a) additional weight (b) recorded error (c) thickness error

Figure 7: Additional weight and measured imperfection

2.2.3. Material properties

Table2 summarized the results of material testing; these represent the average of the values of obtained for three objects. In addition, the obtained mechanical properties are used in the post test simulation presented below.

Table 2 Mechanical properties used in the simulation

mortar		reinforcing bars	
Young's modulus	19663N/mm^2	Young's modulu	204000N/mm^2
Poisson's ratio	0.167	Poisson's ratio	0.3
compressive strength	34.55N/mm^2	yielding point	563.73N/mm^2
tensile strength	3.46N/mm^2		

3. EXPERIMENTAL RESULTS AND POST-TEST ANALYSIS

In the experiment, additional weights were installed first, the sweep examination was performed thereafter, and seismic waves were continuously inputted with two levels of acceleration, as shown in Fig. 8.

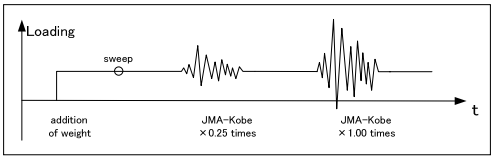

Figure 8: Shaking table test: sequence

3.1. Measurement

Accelerometers were installed on the shaking table, at the locations of the estimated modal peaks, and at the apex, as shown in Fig. 9(a). At the two points of the modal peaks, the strains on the outer and inner surfaces of the concrete and two reinforcing bars were measured, as shown in a figure (b).

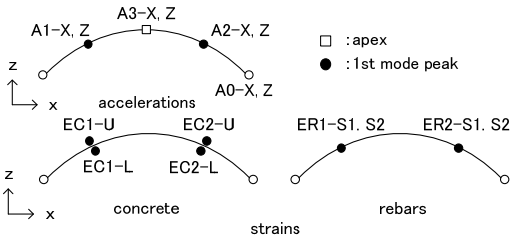

Figure 9: Measurement points of accelerations and strains

3.2. Eigen frequencies

The eigen frequencies obtained by an eigen value analysis and a sweep test are listed in Table 3.

Table 3 Eigen frequencies

		test	pre-test	post-test analysis	
				perfect	imperfect
1st	natural freq. (Hz)	3.22	4.71	4.57	4.85
	narutal period (s)	0.31	0.21	0.22	0.21

As a cause due to which the natural period determined from the sweep test exceeds the computational result, the rigidity reduction caused by the generating of cracks due to the installation of weights and the method of conducting the sweep test can be considered.

3.3. Response time histories

Before the shaking test, when the additional weights were installed, some small cracks were observed near the apex and the support ends. Cracks were observed in the entire arch at the stage of 0.25-times JMA-

Kobe wave input. Subsequently, generation of structural instability was estimated in the case of 1.0-times JMA-Kobe input by the pre-test simulation; in the experiment, destruction occurred similarly. The response time histories of the mode peak (A2) during 1.0-times JMA-Kobe input are shown in Figs. 10 and 11 in comparison with the post-test simulation results. The displacement values in the displacement time history determined from the experiment are calculated by numerical integration of the measured acceleration. In addition, as the input seismic waves in the numerical analyses, the acceleration time history measured on the vibration table was used

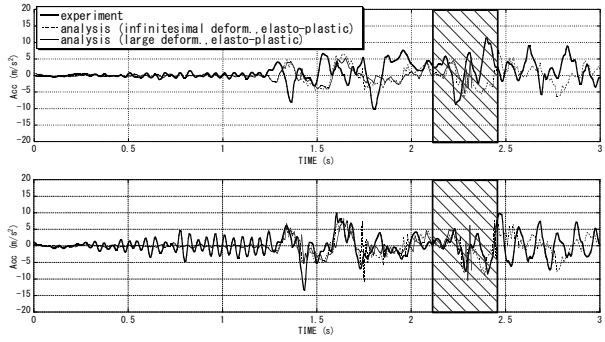

Figure 10: Acceleration time histories

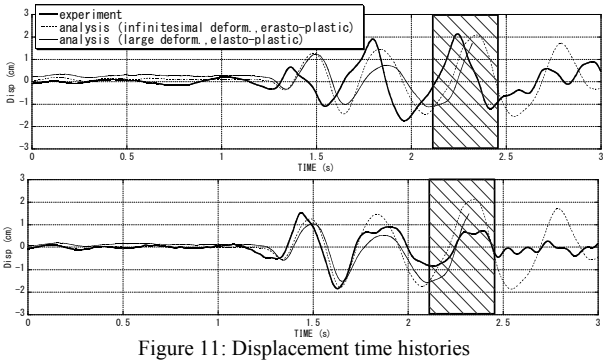

Figure 11: Displacement time histories

In the experiment, it is hard to accurately judge the time when the destruction of the arch occurred from the time history by an accelerometer. However, when analyzed from the video recorded, the time was identified to be in the time zone (2.1 to 2.5 s) shown by shading in Figs. 10 and 11. This result indicates good correspondence to be the instability generation time estimated by the numerical analysis using the dynamic combined nonlinear analysis technique for an RC shell [1-3].

3.4. Failure modes

As seen from the deformation at the time of destruction, shown in Fig. 12, a hinge has occurred on the right-hand side of the specimen. In this test, one hinge is generated which has small domain, and it has not resulted in the structural instability of the entire arch. This is considered to depend, since falling of additional weights was prevented for safety during the experiment.

Figure 12: Dynamic failure in the test.

The deformation mode at the time of a collapse generating assumed by the dynamic analysis is shown in Fig. 13 and "point i" corresponds to the hinge generated in the experiment.

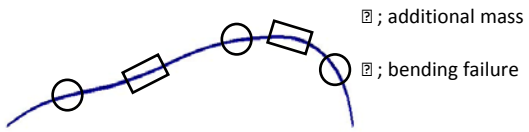

Figure 13: Dynamic failure in the test (enlarged 10 times)

The M-N interaction time histories to the failure estimated by the numerical analyses are shown in Fig. 14. The thick solid lines in the figure show the failure envelope of the RC column, which has the same section as does the target arch. According to these results, the criterion for the dynamic failure of this arch is affected by the influence of geometric nonlinearity. Moreover, this criterion shows the possibility of expressing failure simply by the M-N interaction of an RC column by taking a large deformation into consideration.

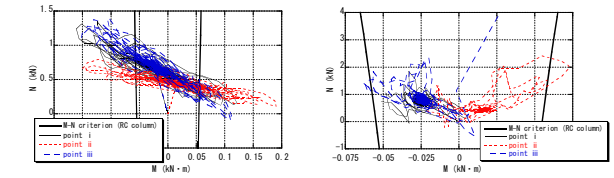

(a) combined nonlinear trajectory (b) linear elastic trajectory

Figure 14: Estimated M-N interaction

4. REINFORCEMENT USING CARBON FIBER SHEET

In this study, dynamic destructive tests were done in the comparison with the RC and the carbon fiber reinforced RC(CFRC) arches.

4.1. Installation of a Carbon Fiber Sheet

The carbon fiber sheet was stuck on the inner circumference side of RC arch with adhesives as shown in Fig. 15.

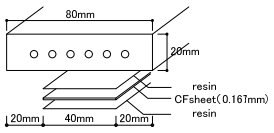

Figure 15: Adhesion of a carbon fiber sheet

Table 4 Material properties of a carbon fiber sheet

density [g/mm2]	tensile strength [N/mm2]	Young's Modulus [N/mm2]	thickness [mm]
0.0003	3400	2.30×10^5	0.167

4.2. Dynamic destruction tests by sweep test

In the dynamic destructive tests, increasing forced excitation tests were done using the resonance frequencies obtained by the sweep test in each step. Estimated initial eigen frequencies and the changes of the resonance frequencies are shown in Table 5 and Fig. 12. In the tests, It was shown that the initial eigen frequency can change with carbon fiber sheets about 50%, and can be controlled widely to RC arch.

Table 5 Initial eigen frequencies (1-st mode)

	sweep test	simulation
	resonance freq.	eigen freq.
RC	5.87 Hz	6.25 Hz
CFRC	9.06 Hz	9.99 Hz

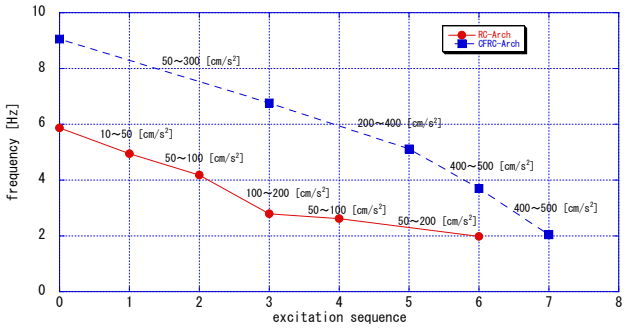

Figure 17: Change of Reconance frequencies

4.3. Difference in damage, response and failure mode

Damage to the RC and CFRC arches in front of destructions are shown in Fig. 18 and 19, respectively. In the RC arch, although progress of cracks is observed on both sides, on the other hand in a CFRC arch, it is not observed in an inner circumference side. The reinforcement by a carbon fiber sheet shows that it is directly effective in prevention of exfoliation of concrete.

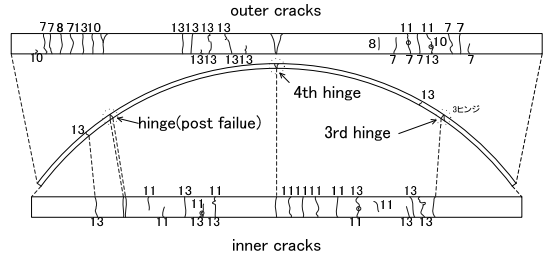

Figure 18: RC arch

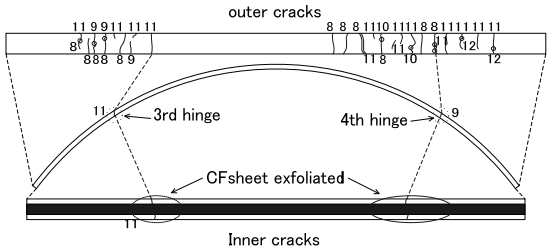

Figure 19: CFRC arch

The acceleration, displacement and rebar strain time histories in the 1-st mode peak point are shown in Fig. 20 and 21 in comparison with RC and CFRC arches. In order to study the responses of the arches in front of destructions, acceleration input were controlled with about 2 Hz(resonance frequency) and 200～300 cm/s^2. Just before destruction of both RC arch and CFRC arches, maximum acceleration showed about 800 cm/ s^2 and the maximum displacement showed about 5 cm. When the maximum of rebar strain response is compared, about 500 micro is shown in RC arch, about 300 micro is shown in a CFRC arch, and the control effect by a carbon fiber sheet is appears.

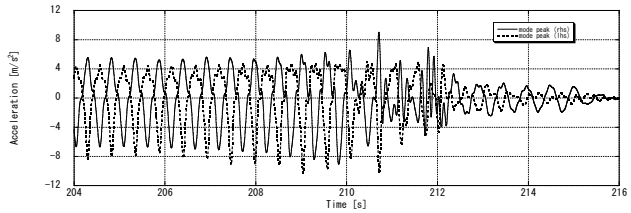

(a)acceleration time histories (Z-dir)

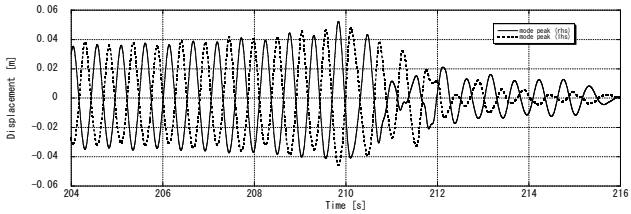

(b)displacement time histories (Z-dir)

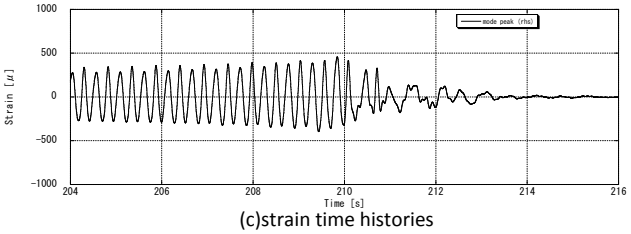

(c)strain time histories

Figure 20: Response time histories（RC arch）

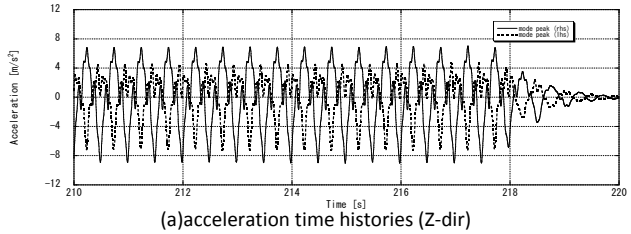

(a)acceleration time histories (Z-dir)

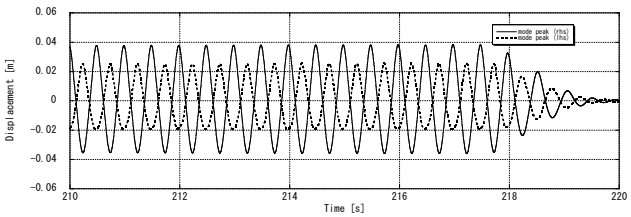

(b)displacement time histories (Z-dir)

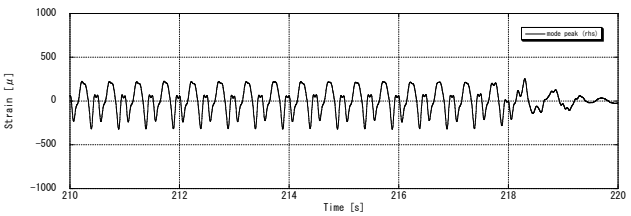

(c)strain time histories

Figure 21: Response time histories（CFRC arch）

Collapse modes of RC and CFRC arch are shown in Fig. 22 with the photographs immediately after the destruction which prevented perfect crash. In RC arch, at the time of about 300 cm/s^2 input, the 3rd hinge and the 4th hinge continued and occurred and failure in brittleness. On the other hand, in the CFRC arch, while CF sheet exfoliated near the primary mode peak point at the time of about 500 cm/s^2 input, the 3rd hinge was formed. , the 4th hinge was formed and by making it resonate compulsorily over two or more times. Then, although the 4th hinge was formed and it became unstable by making it resonate compulsorily over two or more times, perfect crash was not seen and showed the very toughness action.

(a) RC arch (b) CFRC arch

Figure 22: Collapse mode

5. CONCLUSIONS

In this research, the dynamic destructive experiment for RC arch is conducted, and the possibility of pursuit of the phenomenon to a dynamic failure state is verified by the numerical analysis verification. From the obtained experimental results, the dynamic failure mode and the strength of the arch were determined, and a qualitatively and quantitatively good coincidence with the numerical simulation was obtained. It is considered that failure prediction with sufficient accuracy is practically possible. From the obtained results of reinforcing by the carbon fiber sheet, the possibility of control of the natural frequency, reduction of distortion of a steel bars, prevention of exfoliation of inside concrete, and improvement in the toughness at the time of destruction were checked.

6. ACKNOWLEDGEMENTS

This study was supported by the joint research project "NDRR" of Meijo University.

7. REFERENCES

[1] Mutoh A., Kato S. and Matsuoka O., A study on the nonlinear response of RC spherical shells under seismic loading, Proc. Int'l Symposium on Theory, Design and Realization of Shell and Spatial Structures, Int'l Association for Shell and Spatial Structures (IASS), 2001, pp.1-8 (published on CD-ROM), Printed Extended Abstracts: pp.58-59.

[2] Mutoh A., Study on nonlinear vibration characteristics of reinforced concrete spherical shells with fixed load. J. Struct. Constr. Eng., AIJ, 2001; 549:83-90.

[3] Mutoh A., Evaluation of Nonlinear Behavior of Reinforced Concrete Free-Curved Shells Proposed in Recent Years, Proc. Int'l Symposium on Spatial Structures - Permanent and temporary, Int'l Association for Shell and Spatial Structures (IASS), 2010, (published on CD-ROM).

8. APPENDIX

A response analysis method considering geometrically and materially nonlinear analysis based on the FEM is used; the governing equation of motion at time station n+1 is given as

$$\mathbf{M}\ddot{\mathbf{x}}_{n+1} + \mathbf{p}_{n+1} = \mathbf{f}_{n+1} \tag{A1}$$

where M, p, f and x denote the mass matrix, internal resisting forces, external force vector, and nodal displacement, respectively. This problem is dependent on the hysteresis due to concrete cracking/crushing and rebar yielding. The tangential stiffness matrix, the mass matrix and internal resisting force are described as (A2). Here, Rayleigh-type damping is used as shown in this equation.

$$\mathbf{K}_{n+1} = \partial\ \mathbf{p}_{n+1}/\partial\ \mathbf{x}_{n+1} \quad , \quad \mathbf{C}_{n+1} = \partial\ \mathbf{p}_{n+1}/\partial\ \dot{\mathbf{x}}_{n+1}$$
$$\mathbf{p}_{n+1} = \mathbf{C}_{n+1}\ \dot{\mathbf{x}}_{n+1} + \mathbf{K}_{n+1}\mathbf{x}_{n+1} = (\alpha_0\mathbf{M} + \beta_0\mathbf{K}_{n+1})\dot{\mathbf{x}}_{n+1} + \mathbf{K}_{n+1}\mathbf{x}_{n+1} \tag{A2}$$

The external force vector will be shown as follows by assuming multi-directional seismic load and general external force.

$$\mathbf{f}_{n+1} = -\mathbf{M}\ \xi\ \ddot{\mathbf{g}}_{n+1} + \mathbf{b}_{n+1}\ ,\ \ddot{\mathbf{g}}_{n+1} = \begin{Bmatrix} \ddot{\mathbf{g}}^x_{n+1} \\ \ddot{\mathbf{g}}^y_{n+1} \\ \ddot{\mathbf{g}}^z_{n+1} \end{Bmatrix}\ ,\ \xi = \begin{bmatrix} 1 & 0 & 0 \\ 0 & 1 & 0 \\ 0 & 0 & 1 \\ \vdots & & \end{bmatrix} \tag{A3}$$

In this study, the elements considered are the 8-node degenerate shell elements of the popular isoparametric family as shown in Fig.A-1. In the computation, the element is subdivided into equivalent concrete and steel layers across the thickness. A Total Lagrangian approach is employed to describe large deformation problems. In the analysis method, strain and stress were respectively made to be Green-Lagrange strain and 2nd Piola-Kirchhoff stress. The strain-displacement and stress-strain relations are given by

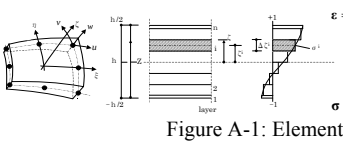

$$\boldsymbol{\varepsilon} = \{\partial u/\partial x, \partial v/\partial y, \partial u/\partial y + \partial v/\partial x, \partial u/\partial z + \partial w/\partial x, \partial v/\partial z + \partial w/\partial y\}^T + \left\{\frac{1}{2}\left(\frac{\partial w}{\partial x}\right)^2, \frac{1}{2}\left(\frac{\partial w}{\partial y}\right)^2, \frac{\partial w}{\partial x}\frac{\partial w}{\partial y}, 0, 0\right\}^T \tag{A4}$$
$$\boldsymbol{\sigma} = \{\sigma_x, \sigma_y, \tau_{xy}, \tau_{xz}, \tau_{yz}\}^T$$

Figure A-1: Element geometry

While to considering concrete cracking (open/close), crushing and rebar yielding, the incremental theory of plasticity was adopted for the analysis. The uniaxial stress-strain relations of a concrete and a steel bar are shown in Fig.A-2. The assumed biaxial strength envelope for plain concrete is modelled based on Kupfer's results [6] as shown in Fig.A-3. In the numerical simulation, a constant value of 0.25 has been used as the shear retention factor of cracked concrete. In this study, elastic unloading and re-loading are assumed in the cyclic loading in order to ensure stability in the numerical calculation.

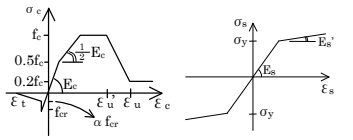

Fig. A-2: Stress-strain relation

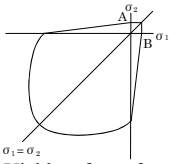

Fig. A-3: Yield surface of concrete

In the computation, the yield functions of concrete are modelled in Eqs.(A6) and (A7).

(biaxial compressive stress state)

$$f(\boldsymbol{\sigma}) = \left\{1.355\left[\left(\sigma_x^2 + \sigma_y^2 - \sigma_x^2\sigma_y^2\right) + 3\left(\tau_{xy}^2 + \tau_{xz}^2 + \tau_{yz}^2\right)\right] + 0.355 f_c\left(\sigma_x + \sigma_y\right)\right\}^{1/2} = f_c \tag{A6}$$

(compression-tension stress state)

$$f(\boldsymbol{\sigma}) = \frac{\left(f_c - f_{cr}\right)\left(\sigma_m - \sqrt{J_2}\sin\phi/\sqrt{3}\right)}{f_c + f_{cr}} + \sqrt{J_2}\cos\phi - \frac{f_c f_{cr}}{f_c + f_{cr}} \tag{A7}$$
$$\sigma_m = \frac{1}{3}\left(\sigma_x + \sigma_y + \sigma_z\right) \quad J_2 = \frac{1}{3}\left(\sigma_x^2 + \sigma_y^2 - \sigma_x\sigma_y\right) + \tau_{xy}^2 \quad \phi = \frac{1}{3}\sin^{-1}\left\{-\frac{3\sqrt{3}J_3}{2(J_2)^{3/2}}\right\}$$
$$J_3 = -\frac{1}{27}\left(2\sigma_x - \sigma_y\right)\left(2\sigma_y - \sigma_x\right)\left(\sigma_x + \sigma_y\right) + \frac{1}{3}\left(\sigma_x + \sigma_y\right)\tau_{xy}^2$$